Fractal kinetics of radiation-induced point-defect formation and decay in amorphous insulators: Application to color centers in silica-based optical fibers

David L. Griscom*
Optical Sciences Division, Naval Research Laboratory, Washington DC 20375
(Received 23 April 2001; published 3 October 2001)

Formalisms have been developed to express the time evolution of bimolecular processes taking place in fractal spaces. These ''stretched-second-order'' solutions are specifically applicable to radiation-induced electron-hole pairs and/or vacancy-interstitial pairs in insulating glasses. Like the analogous Kohlrausch-type (stretched-first-order) expressions, the present solutions are functions of $(kt)^{\beta}$, where $0<\beta<1$, k is an effective rate coefficient, and t is time. Both the new second-order formalism and the familiar Kohlrausch approach have been used to fit experimental data (induced optical absorptions in silica-based glasses monitored at selected wavelengths) that serve as proxies for the numbers of color centers created by γ irradiation and/or destroyed by processes involving thermal, optical, or γ-ray activation. Two material systems were investigated: (1) optical fibers with Ge-doped-silica cores and (2) fibers with low-OH/low-chloride pure-silica cores. Successful fits of the growth curves for the Ge-doped-silica-core fibers at four widely separated dose rates were accomplished using solutions for color-center concentrations, $N[(kt)^{\beta}]$, which approach steady-state values, N_{sat}, as $t\rightarrow\infty$. The parametrization of these fits reveals some unexpected, and potentially useful, empirical rules regarding the dose-rate dependences of β, k, and N_{sat} in the fractal regime $(0<\beta<1)$. Similar, though possibly not identical, rules evidently apply to color centers in the pure-silica-core fibers as well. In both material systems, there appear to be fractal$\Leftrightarrow$ classical phase transitions at certain threshold values of dose rate, below which the dose-rate dependencies of k and N_{sat} revert to those specified by classical $(\beta=1)$ first- or second-order kinetics. For $kt\ll 1$, both the first- and second-order fractal kinetic growth curves become identical, i.e., $N((kt)^{\beta})\approx At^{\beta}$, where the coefficient A depends on dose rate but not kinetic order. It is found empirically that A depends on the $3\beta/2$ power of dose rate in both first- and second-order kinetics, thus ''accidentally'' becoming linearly proportional to dose rate in cases where $\beta\approx 2/3$ (characteristic of random fractals and many disordered materials). If interfering dose-rate-independent components are absent, it is possible to distinguish the order of the kinetics from the *shapes* of the growth and decay curves in both fractal and classical regimes. However, for reasons that are discussed, the parameters that successfully fit the experimental growth curves could not be used as bases for closed-form predictions of the shapes of the decay curves recorded when the irradiation is interrupted.

DOI: 10.1103/PhysRevB.64.174201 PACS number(s): 61.72.Ww, 61.43.Fs

I. INTRODUCTION

Due mainly to continuing needs to deploy optical fibers in both high- and low-dose-rate radiation environments there has been an unabating interest in understanding the kinetics of color center formation (more precisely, the interplay of creation and annihilation mechanisms) and of their thermally activated decays when the irradiation is interrupted.[1–11] The decay kinetics of radiation-induced attenuation in optical fibers has been variously fitted by power laws,[6] high-order kinetic solutions[8] $(n\geq 2)$ or more *ad hoc* expressions.[7] In other glasses, the concentrations of color centers have been measured directly by electron spin resonance and their thermal decays have been fitted[12] by the ''stretched exponential'' Kohlrausch function,[13–15]

$$N(t)=N(0)\exp[-(t/\tau)^{\beta}], \tag{1}$$

where $N(t)$ is the number density of color centers, τ is the characteristic decay time, and β is a number between 0 and 1. The possible underlying physical meanings of the fractional exponent β are many and various, although they generally fall into one of two categories: (i) those ascribed to diffusion-controlled reactions involving the concept of dispersive transport in disordered structures and (ii) those based on the model of hierarchically limited dynamics resulting in correlated relaxation processes consisting of several successive steps.[16] It seems likely that color center formation and decay in glasses is an example of the former.

Derivation of Eq. (1) begins with the classical first-order rate equation

$$dN(t)/dt=-RN, \tag{2}$$

where $R(=1/\tau)$ is the decay rate constant. The Kohlrausch solution, Eq. (1), is the result of the change of dimensionless variable $Rt\rightarrow(Rt)^{\beta}$, $0\leq\beta\leq 1$, which transforms Eq. (2) to $dN[(Rt)^{\beta}]/d(Rt)^{\beta}=-N$. The rate equation for this case can also be written in the form $dN/dt=-R(t)N$, where the time-dependent relaxation ''coefficient'' $R(t)$ is given by $(\beta R^{\beta}/t^{1-\beta})$ and R is the classical (time-independent) rate constant. Applied to category-(i) processes, the (nonexponential) result of Eq. (1) is generally viewed as a mathematically convenient approximation to the net result of a weighted superposition of the contributions of a range of classical exponential relaxation processes

$$N(t)=\int_0^\infty \phi(R)\exp(-Rt)dR, \tag{3}$$

where the weighting function $\phi(R)$ represents a normalized distribution of reaction rates.

The growth curves experimentally recorded for color center formation in glasses during irradiation (e.g., induced attenuation in optical fibers as a function of accumulated dose D) very commonly take the form of power laws that prevail over several decades in the value of D:[8–10]

$$N(t)=C(\dot{D}t)^f, \tag{4}$$

where $\dot{D}$ is the dose rate and C is a parameter that may or may not depend on $\dot{D}$. Griscom, Gingerich, and Friebele[9] provided a heuristic demonstration that any such power-law growth curve can be deconstructed into a weighted superposition of saturating classical nth order kinetic growth processes proceeding in parallel, in analogy to the way that Eq. (3) may provide the physical explanation of the decay curves.

Mashkov *et al.*[17] appear to have been the first to derive closed-form Kohlrausch-type solutions for color-center-center *creation* that reproduce the observed power-law growth curves in the low-dose regime before saturation sets in. Specifically, these authors considered the set of *first-order* defect processes indicated by the diagram,

$$n_0 \xrightarrow{k_c} d \underset{k_d}{\overset{k_a}{\leftrightarrows}} p, \tag{5}$$

where n_0 represents the number density of damageable sites in the undamaged glass network, d the number density of color centers [i.e., $N(t)$ in present notation], and p the number density of color center precursors (e.g., neutral oxygen vacancies in glassy SiO_2). The rate constant k_c governs the creation of new color centers (e.g., by oxygen displacements and concurrent trapping of a hole at the vacancy site) while the rates k_a and k_d pertain to the activation and deactivation, respectively, of color center precursors (e.g., respectively trapping and detrapping holes on oxygen vacancies). The classical first-order kinetic equations expressing the processes of scheme (5) were presented as[17]

$$dN/dt=k_c\dot{D}N_0+k_a\dot{D}N_p-k_d\dot{D}N \tag{6}$$

and

$$dN_p/dt=k_d\dot{D}N-k_a\dot{D}N_p\,. \tag{7}$$

Here, N_0 was stated to represent the number density of network sites where defects can be created (e.g., the number of bridging oxygens that can be displaced to form a vacancy). Since it was presumed that $N \ll N_0$ for all practical radiation doses, N_0 is essentially a constant and could well be subsumed into k_c. Elsewhere in the present paper a hybrid option is adopted, namely, N_0 is replaced by N^*, where the latter is defined to have unit magnitude but retains the dimensionality of the color center number density (e.g., cm^{-3} or g^{-1}). This artifice seems to improve the transparency of the changes of dimensionless variables required to obtain stretched kinetic solutions.

With regard to Eqs. (6) and (7), Mashkov *et al.*[17] used the change of variable,

$$k\dot{D}t\rightarrow(k\dot{D}t)^\beta\equiv\xi, \quad 0\leqslant\beta\leqslant1, \quad k=k_a+k_d, \tag{8}$$

resulting in a new set of kinetic equations taking the same form as Eqs. (6) and (7) except that the left-hand sides were replaced by $dN/d\xi$ and $dN_p/d\xi$, respectively. It was then necessary to determine the relationships of the parameters on the right-hand sides of the new equations to those of the right-hand sides of Eqs. (6) and (7). For purposes of this brief summary, these details are omitted and only the solution of Mashkov *et al.* for the number of activated color centers is reproduced here:[17]

$$N(D)=N_c(kD)^\beta+N_a\{1-\exp[-(k\dot{D}t)^\beta]\}, \tag{9}$$

where $N_c=(k_c/k)^\beta(k_a/k)N_0$ and $N_a=(k_c/k)^\beta(k_d/k)N_0+(k_a/k)N_p(0)$. The first term on the right-hand side of Eq. (9) represents ''unlimited'' (so long as $N \ll N_0$) creation of new defects from the glass network and their concurrent activation, while the second term represents the activation of a fixed number of preexisting precursors $N_p(0)$, limited by radiation-stimulated deactivation. Mashkov *et al.*[17] applied Eq. (9) to the case of E' centers (a positively charged oxygen vacancy defect detected by electron spin resonance) in two types of fused silica, successfully fitting the growth curves for the number densities of these color centers over more than four decades of dose.

It is remarked that Eqs. (6) and (7) are based exclusively on (a) first-order kinetics and (b) decay rate parameters that assume that radiation-stimulated back reactions are the only mechanisms of color-center destruction. By contrast, kinetic processes involving *thermally* activated recombinations of vacancies and interstitials and/or electrons and holes ought to be second-order processes. And, whatever the governing kinetic order, most data for radiation-induced color centers in silica-based fiber optics in fact exhibit thermally activated decay modes that are responsible for the fading observed when the radiation is interrupted and no bleaching light is being propagated.[1,2,7–9] Therefore, Sec. II presents three new ''stretched'' kinetic formulations based on thermal decay processes, which are then tested in Sec. IV by fitting data for induced attenuation of light in Ge-doped-silica-core optical fibers recorded as functions of time during and after irradiation by γ rays.[18] Some surprising empirical rules for the dose-rate dependences of the kinetic coefficients are determined in this process, but not before consideration was paid to the possibility that the optically dominant thermally-decaying defect population (termed ''Population *A*'') is in each case accompanied by one or more nondecaying components (Populations *B*, *C*, etc.) that account for a relatively weak dose-rate-independent ''background.'' In Sec. V, attempts are made to apply the present formalisms to approximate the more complex kinetics of color-center creation in

pure and fluorine-doped silicas[19–21] by γ irradiation and the bleaching of these centers by thermal, optical, and radiation-stimulated processes.

II. OTHER STRETCHED KINETIC FORMALISMS

a. First-order growth kinetics with thermally activated decay. The classical rate equation for this situation can be written as

$$dN(t)/dt = K\dot{D}N^* - RN, \tag{10}$$

and its solution is given by

$$N(t) = N_{\text{sat}}\{1 - \exp[-Rt]\}, \tag{11}$$

where $N_{\text{sat}} = (K\dot{D}/R)N^*$. Making the change in dimensionless variable $kt \rightarrow (kt)^{\beta}$ leads to the new rate equation,

$$dN[(kt)^{\beta}]/d(kt)^{\beta} = (K\dot{D}/R)^{\beta}N^* - N, \quad 0 < \beta < 1, \ k = R, \tag{12}$$

with solution

$$N[(Rt)^{\beta}] = n_{\text{sat}}\{1 - \exp[-(Rt)^{\beta}]\}, \tag{13}$$

where $N_{\text{sat}} = (K\dot{D}/R)^{\beta}N^*$. Note that for $Rt \ll 1$, Eq. (13) reduces to the power law of Eq. (4) if $f = \beta$ and $C = K^{\beta}N^*$.

b. Second-order growth kinetics with thermally activated decay. The classical rate equation for this situation can be written as

$$dN(t)/dt = K\dot{D}N^* - RN^2/N^*, \tag{14}$$

and its solution is given by

$$N(t) = N_{\text{sat}} \tanh(kt), \tag{15}$$

where $N_{\text{sat}} = (K\dot{D}/R)^{1/2}N^*$ and $k = (K\dot{D}/R)^{1/2}$. The ''stretched'' version of second-order growth kinetics is accomplished by the change in dimensionless variable $kt \rightarrow (kt)^{\beta}$, leading to the new rate equation

$$dN[(kt)^{\beta}]/d(kt)^{\beta} = (K\dot{D}/R)^{\beta/2}N^* - (R/K\dot{D})^{\beta/2}N^2/N^*,$$

$$0 < \beta < 1 \quad k = (K\dot{D}R)^{1/2} \tag{16}$$

with solution

$$N[(kt)^{\beta}] = N_{\text{sat}} \tanh[(kt)^{\beta}], \tag{17}$$

where $N_{\text{sat}} = (K\dot{D}/R)^{\beta/2}N^*$. As in the case of the saturating stretched exponential [Eq. (13)], the saturating second-order growth function of Eq. (17) also reduces to the power law of Eq. (4) for $kt \ll 1$, by making the definitions $f = \beta$ and $C = K^{\beta}N^*$.

c. Thermally activated second-order decay kinetics. The classical rate equation for second-order decays in the absence of continuous creation is given by Eq. (14) for the case $K = 0$. Its solution is

$$N(t) = N(0)\{1 + [N(0)/N^*]Rt\}^{-1}, \tag{18}$$

where $N(0)$ is viewed as the number of color centers present at the instant the irradiation is stopped. Change of the dimensionless variable $Rt \rightarrow (Rt)^{\beta}$ results in the new rate equation

$$dN[(Rt)^{\beta}]/d(Rt)^{\beta} = -N^2/N^*, \quad 0 < \beta < 1 \tag{19}$$

with solution

$$N[(Rt)^{\beta}] = N(0)\{1 + [N(0)/N^*](Rt)^{\beta}\}^{-1}. \tag{20}$$

III. EXPERIMENTAL DETAILS

A. Ge-doped-silica-core fibers

The Corning SMF-28 single-mode (SM) and 62.5/125 multimode (MM) optical fibers employed in this study both comprised GeO_2-doped-amorphous-SiO_2 cores with pure-silica optical claddings and polymer protective jackets. Test fibers of suitable lengths (10–100 m, depending on radiation sensitivity) were wound on paper forms and placed in a watertight stainless steel can for insertion into the Naval Research Laboratory (NRL) ^{60}Co underwater γ-ray source. Dose rates of 340, 17, and 0.45 rad/s were selected by locating the can at appropriate distances from the source. Separate samples of the same fiber types were also subjected to long-term irradiation at a fission reactor at a dose rate of 0.000 88 rad/s, and one SM fiber was exposed to a low-activity γ ray source at a dose rate of 0.011 rad/s. In all cases reported here the sample container was equipped with a resistive heater and a thermocouple for maintaining the temperature at 50 °C. Leads from the experimental fiber coils were conducted through a seal at the top of the container and fusion spliced to 7 m lengths of the same fiber type leading to the light sources (LED's, light-emitting diodes) and detectors. To compensate for any fluctuations in source power, fiber beam splitters were used to divide the light from the LED's into sample and reference channels that were monitored separately. To minimize photobleaching, sample-channel powers were limited to $\leqslant 1$ μW. The data to be shown were acquired at a wavelength of 1.3 μm during simultaneous irradiations of the MM and SM Corning fibers. Additional details are provided elsewhere.[18]

B. Pure and F-doped silica-core fibers

The core materials for the two multimode test fibers were (1) Russian-developed KS-4V silica containing $<$200 ppb OH and $<$20 ppm Cl and (2) a vapor-axially deposited silica of Japanese origin containing $\sim$0.54 mass% F and $\sim$4 ppm OH. Both of these fibers had F-doped-silica optical claddings and aluminum protective jackets. Experimental fibers consisted of ''sample lengths'' of 1, 4 or 10 m coiled under zero tension to diameters of 62 mm and 10-cm ''reference lengths'' at the irradiation position; integral 8-m pigtails extended from these to the light source and spectrometer. The NRL ''swimming pool'' ^{60}Co γ ray source was used for all irradiations in the manner prescribed in Sec. III A. As described elsewhere,[19] induced absorption spectra in the wavelength range $\sim$400–1000 nm were developed from transmitted spectral intensities dispersed by a prism onto a charge-coupled-device (CCD) camera. A few spectra extending from

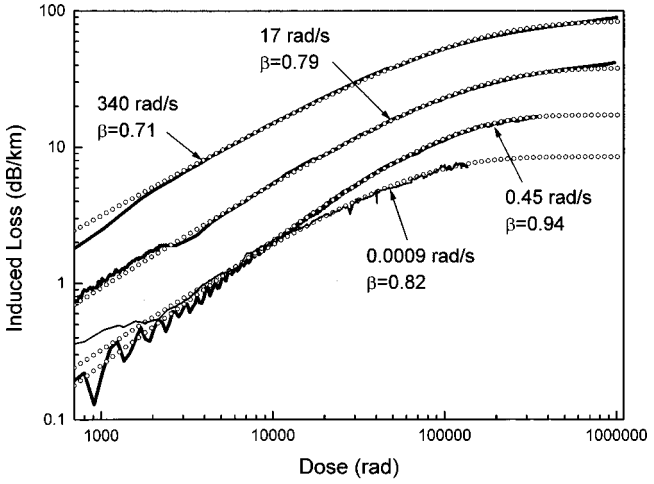

FIG. 1. Growth of induced attenuation at 1300 nm in Corning MM Ge-doped-silica-core fiber subjected to γ irradiation at dose rates of 0.45, 17, and 340 rad/s and reactor at 0.000 88 rad/s. All irradiations were carried out at 50 °C. Solid curves are the experimental data; small circles are fits to these data based on the stretched first-order-kinetic growth solution, Eq. (13), using the parameters plotted in Fig. 2 as open circles. Comparable fits using the stretched second-order solution, Eq. (17), and the parameters plotted in Fig. 2 as solid squares were also achieved but are not shown.

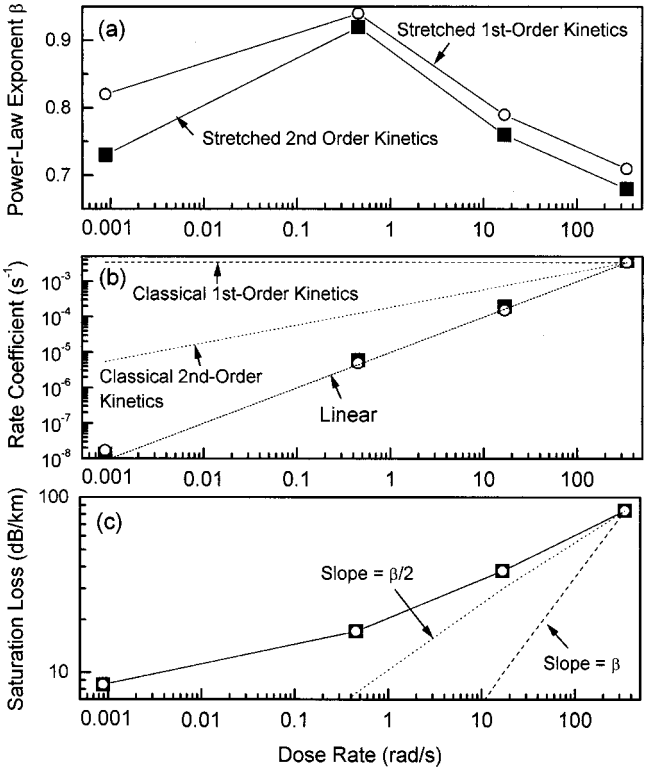

FIG. 2. Best-fit parametrizations of Eqs. (13) [open circles] and (17) [solid squares] used in simulations of the experimental growth curves of Fig. 1. Dashed and dotted lines in (b) portray the expected behaviors if the data were to obey classical first- and second-order kinetics, respectively.

400 to 1500 nm were recently recorded on an optical signal analyzer (OSA). Data were acquired during γ irradiation at 27 °C and several brief periods of time out of the source (at ~20 °C). In the case of the prism spectrometer, probe light from a quartz-tungsten-halogen lamp was launched into each sample/reference pair via a 1×2 fiber-optic coupler (~5 μW/fiber) and the lamp was turned on for ~2–5 s per frame grab except during a separate optical bleaching experiment. Exposure times ~0.2–0.5 s possible with the CCD camera assured precise time tagging of these spectral data. In the case of spectra recorded on the OSA, the launched light intensity was ~10 μW and the duration of illumination was >20 s, the length of time required to complete a signal-averaged spectral scan.

IV. STRETCHED KINETIC FITS OF DATA FOR Ge-DOPED-SILICA-CORE FIBERS: ELUCIDATION OF EMPIRICAL RULES FOR DEFECT CREATION IN FRACTAL SPACES

A. Growth curves

a. Multimode fiber. Figure 1 illustrates the growth of optical attenuation in the MM fiber measured during ^{60}Coγ irradiation at three different dose rates and reactor irradiation at a fourth, lower dose rate. The small open circles are fits to the data achieved using the ''stretched saturating exponential'' solution, Eq. (13). Figure 2 (open circles) displays the corresponding fitting parameters as a function of dose rate. Comparable fits to the same data (not shown) were also achieved using the ''stretched second-order'' solution of Eq. (17); the fitting parameters in the latter case are shown by the solid squares in Fig. 2. It is striking that the parameters of the two fits are essentially identical despite the differing meanings of the rate coefficients [$k=R$ in Eq. (13) vis-à-vis $k=(K\dot{D}R)^{1/2}$ in Eq. (17)]. Nevertheless, this result is expected, given that both solutions when expanded as power series have identical lowest-order terms, i.e., $N[(\dot{D}t)^{\beta}]\approx(K\dot{D}t)^{\beta}$ in the limit $kt\ll1$ for both $n=1$ and $n=2$ stretched kinetic formulations.

In Fig. 2(c) the values of $N_{\rm sat}$ were deliberately constrained to be identical for both the first- and second-order stretched kinetic fits (although they would turn out to be approximately the same in any event). At the highest dose rates, the measured values of $N_{\rm sat}$ approximately follow prediction for the second-order case, i.e., $N_{\rm sat}=(K\dot{D}/R)^{\beta/2}N^*$ if the underlying rate ''constants'' K and R are assumed to be actually independent of dose rate. However, in Fig. 2(b) it is seen that the experimental determinations k are linearly proportional to $\dot{D}$, whereas the classical first- and second-order kinetic solutions, Eqs. (11) and (15), respectively require that $k_{n=1}\equiv R=$const, independent of dose rate, while $k_{n=2}\equiv(K\dot{D}R)^{1/2}$.

It is here postulated that the evident dose-rate dependences of the coefficients K and R in the ''stretched'' kinetic solutions of Eqs. (13) and (17) can be *empirically deduced*, provided that the interfering effects of other possible color-center populations can be minimized. (It is always possible that several overlapping but unrelated optical bands may contribute to the optical losses measured at any given wave-

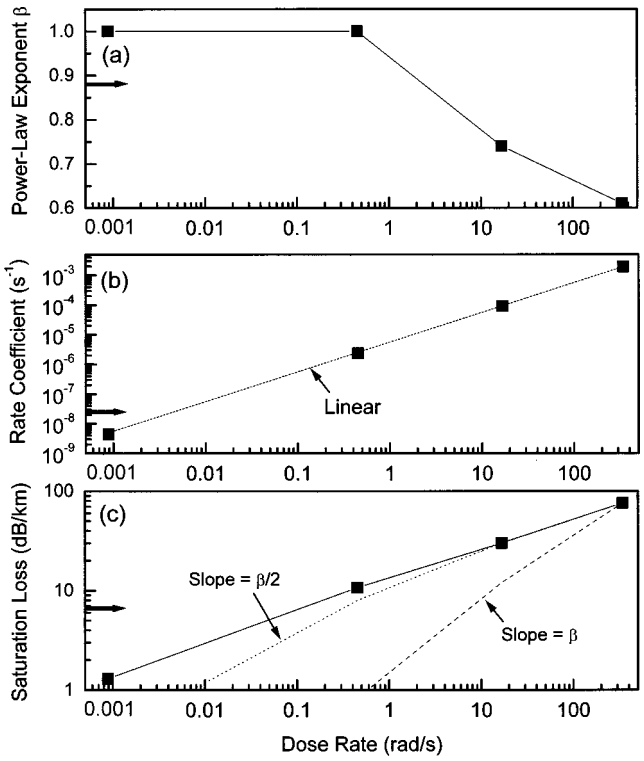

FIG. 3. Best-fit ''Population-*A*'' parameterizations of Eq. (17) [solid squares] used to the fit the data of Fig. 1 under the assumption that a dose-rate-independent ''Population *B*'' also contributes to the experimental growth curves. (The quality of these fits was comparable to those of Fig. 4, but they are not shown.) The Population-*B* parameters (arrows on *y* axes) were optimized on the notional criterion that the Population-*A* values of saturation loss (c) should track a curve with slope $\beta/2$, where β is the best-fit power-law exponent from (d).

length.) Accordingly, the possibility was explored that the experimental values of N_{sat} may define a simple power law of dose rate when proper account is taken of spurious overlapping bands. Specifically, from the concave-upwards aspect of the fitting parameters of Fig. 2(c), it was supposed that the experimental spectra may comprise contributions from *two different* defect populations: (A) a thermally decaying component obeying Eq. (13) or Eq. (17) and (B) a much weaker component ($N_{\mathrm{sat}}^{(B)}<20$ dB/km) arising from dose-rate-independent activation of precursor sites. Successful simulations of the growth curves of Fig. 1 (not shown) were accomplished under this ''two-different-color-center model'' using the parameters of color center ''Population *A*'' shown in Fig. 3 (squares) and those of dose-rate-invariant ''Population *B*'' indicated by the arrows on the *y* axis. By construction, $N_{\mathrm{sat}}^{(A)}$ now very nearly follows a power law of dose rate, specifically $\dot{D}^{\beta/2}$ [Fig. 3(c)]. Notably, in the process of forcing $N_{\mathrm{sat}}^{(A)}$ into a consistent dependence on dose rate, the rate coefficient *k* for Population *A* has converged to a dependence on dose rate that is precisely linear to within the scatter of the cut-and-try fitting attempts [Fig. 3(b)].

The fits whose parameters are plotted in Fig. 3 are based on the second-order formalism of Eq. (17), but given the results of Fig. 2 it is clear that similar results might also have been achieved using the Kohlrausch solution of Eq. (13). So, up to this point, no inferences can be drawn regarding the actual kinetic order. Supposing, for the sake of argument, that the parameters of Population *B* have been ''correctly'' chosen in Fig. 3, let us consider the implications of assuming that we know the correct kinetic order. If second order is assumed to be correct, then the data of Fig. 3(c) show that K/R must be independent of $\dot{D}$, but combining this observation with the data of Fig. 3(b) leads to the conclusion that both *K* and *R* must separately be proportional to $\dot{D}^{1/2}$. On the other hand, if first-order kinetics are assumed to be correct, Fig. 3(b) clearly-shows $R(\equiv k)$ to depend linearly on $\dot{D}$, whereupon the data of Fig. 3(c) and the definition of N_{sat} then demand that *K* be proportional to $\dot{D}^{1/2}$. These empirical inferences are summarized in Table I.

TABLE I. Parameters of the first- and second-order fractal-kinetic solutions of Eqs. (13) and (17), respectively. The empirically inferred relationships are based on data for Ge-doped-silica fibers. (Note that the parameters *K* and *R* are independent of dose rate in classical kinetics.)

	Parameters	
	First-order solution	Second-order solution
Specified by formalism	$k=R$ $N_{\mathrm{sat}}\approx(k\dot{D}/R)^{\beta}$	$k=(K\dot{D}R)^{1/2}$ $N_{\mathrm{sat}}=(K\dot{D}/R)^{\beta/2}$
Empirically inferred	$R\propto\dot{D}$ $K\propto\dot{D}^{1/2}$	K/R independent of $\dot{D}$ $K\cdot R\propto\dot{D}$

As pointed out in Sec. II, the coefficient *C* in the power-law expression of Eq. (4) is given by $C=K^{\beta}N^{*}$ in both the Kohlrausch and stretched-second-order formalisms in the limit $kt\ll 1$. It follows from the empirical deductions of Table I that $C/N^{*}=K^{\beta}\propto D^{\beta/2}$ in both kinetic orders. Therefore, in the short-time limit Eq. (4) can be empirically recast in the form

$$N(t)=C'\dot{D}^{3\beta/2}N^{*}t^{\beta}, \tag{21}$$

where $0<\beta<1$ and C' is a constant independent of both dose rate and kinetic order.

b. Fractal kinetics. The significance of the exponent β is now considered. In classical kinetics, $\beta=1$ and all rate constants are rigorously independent of time. But for reactions taking place in fractal spaces, the rate constants are replaced by rate ''coefficients'' that are found to be time dependent, both experimentally and in computer simulations.[22] [Recall that the rate coefficient in the Kohlrausch solution is given by $R(t)=\beta R^{\beta}/t^{1-\beta}$, where $0<\beta<1$ and *R* is a constant.] Indeed, it has been shown that the Kohlrausch law itself can be derived from a defect-diffusion model in fractal spaces.[23] Fractals differ from Euclidian spaces by having ''fractal dimensions'' $d_f<d$, where *d* is the dimension of the Euclidian space in which the fractal is embedded.[24] Each fractal also possesses a ''spectral dimension'' $d_s(<d_f<d)$, defined by the probability *P* of a random walker returning to its point of origin after time *t*,

$$P(t) \propto t^{-d_s/2}. \tag{22}$$

It is known[25,26] that $d_s \approx 4/3$ for the whole class of random fractals embedded in Euclidian spaces of dimensions $d \geqslant 2$. Random fractals include the percolation cluster, which can be considered as the prototype for the structures of many vitreous materials. As it is used in the present paper, the exponent β corresponds identically to $d_s/2$. Thus, for the percolation cluster, and presumably for many glasses, $\beta \approx 2/3$.

As a corollary, in the case of random fractals, Eq. (21) approximates to $N(t) \approx C' \dot{D} t^{2/3}$, where C' is empirically found to be independent of both dose rate and of kinetic order (at least for $n=1$ and $n=2$). Henschel and Baumann[10] have observed that a family of induced-loss curves measured at $\lambda = 1308$ nm for Ge-doped-silica-core fibers irradiated at dose rates ranging from 0.76 to 122 rad/s could be made to overlay in the power-law regime (in their case $\beta \approx 0.78$) when each curve was divided by the corresponding value of $\dot{D}$ and plotted versus time. These authors correctly noted that this outcome is predicted for both first- and second-order *classical* kinetics ($\beta = 1$) and they puzzled over the apparent applicability of the same rule to cases where the initial growth law is t^{β} $(0 < \beta < 1)$ rather than linear. On the basis of the present empirical rules, it appears that such a linear dependence on dose rate can also be an ''accidental'' property of fractal kinetics in the special case of reactions taking place on random fractals ($\beta \approx 2/3$).

Because all of the data presented here were acquired over only three decades of dose, it was not possible to replicate the ''early-time'' $(kt \ll 1)$ power-law behaviors presented by Henschel and Baumann,[10] whose data extended backwards in time by three more decades. In fact, whereas the latter workers found all of their growth curves for a given fiber type to be characterized by a fixed value of β-independent dose rate, the present results obtained by using either Eq. (13) or Eq. (17) to fit the high-dose parts of the growth curves generally show $\beta \approx 2/3$ at the highest dose rate but $\beta > 2/3$ at lower dose rates. In particular, in Fig. 2(a) the fitted values of β are seen to increase with decreasing dose rate until reaching a cusp and then to decrease to lower values at the lowest dose rate. Intuitively, it would seem more plausible in cases where β increases with decreasing dose rate that once it reaches its classical value of 1.0 it should remain there as the dose rate is lowered further. This conjecture is supported by the ''two-different-color-center-model'' fit whose parameters are represented in Fig. 3. To the extent that the latter fit is valid, it is inferred that the fractal kinetics observed at high dose rates may (at least in the presently investigated fibers) revert to classical kinetics at dose rates below ~0.5 rad/s. But if classical kinetics truly rules this low-dose-rate regime, it would then follow that the underlying rate constants K and R must return to being independent of dose rate. Accordingly, in Fig. 4 the data of Fig. 1 have been refitted by the same two-different-color-center model as for Fig. 3, except that the predicted dose-rate independence of K and R was enforced in the classical regime. Thus, for classical second-order kinetics, $k \equiv (K\dot{D}R)^{1/2}$ and $N_{\mathrm{sat}} \equiv (K\dot{D}R)^{1/2} N^*$ both vary as the square root of dose rate. Under these constraints, the fits of Fig. 4 were accomplished by use of the color-center ''Population-*A*'' kinetic parameters illustrated in Fig. 5 and the dose-rate-independent ''population-*B*'' growth curve illustrated by the solid circles in Fig. 4. It is cautioned that the success of this fit may yet prove fortuitous, since the intensities associated with Population *A* at the lowest dose rate are relatively small compared to the intensities associated with the invoked Population *B*. However, the successful fits to the data of Fig. 4 do uphold the plausibility of there being a classical⇄fractal phase transition at a dose rate ~0.4 rad/s, as suggested in Fig. 5.

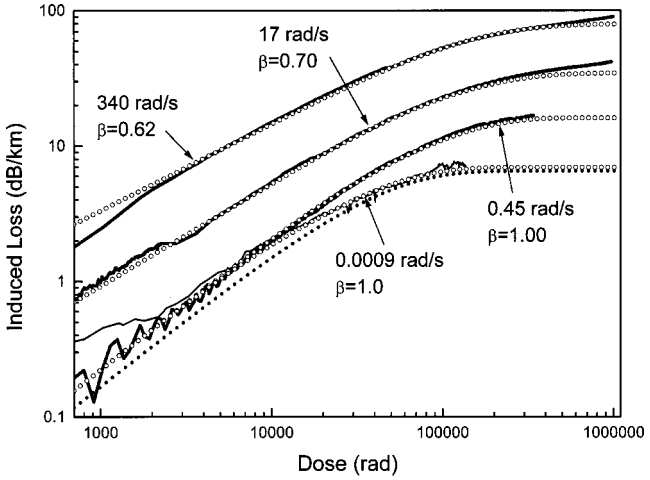

FIG. 4. The same experimental data as displayed in Fig. 1 (solid curves) are here fitted (open circles) by stretched second-order kinetic solution, Eq. (17), using the best-fit Population-*A* parameters shown in Fig. 5, together with the best-fit dose-rate-independent Population-*B* curve plotted in the present figure as solid circles. (For purposes of this simulation, discrepancies between the experimental and simulated curves at highest doses were ignored.)

c. Single-mode fiber. For this study data were available for fibers exposed at five different dose rates, counting both the reactor irradiation and the γ-ray air source. However, it became evident that the reactor and air-source results are incompatible, given that higher dose-for-dose induced losses were recorded in the former case (at 0.000 88 rad/s) than in the latter (at 0.011 rad/s), in contradiction to the empirical dose-rate-dependence rules evolved above [e.g., Eq. (21)]. (The most likely reason for this outcome is that the fibers are in fact more sensitive to the neutron flux of the reactor than has been accounted for by the available dosimetry.) Thus, it would be futile to try to fit all five curves simultaneously. Accordingly, separate fits were carried out on two ensembles of data consisting of (i) the growth curves recorded at the three highest γ-ray dose rates supplemented by the reactor growth curve and (ii) the growth curves recorded at the three highest γ-ray dose rates supplemented by the γ-ray air-source data.

The fits of the SM data ensembles that included the reactor data (not shown) were successfully carried out in much the same manner as the fitting of the MM γ-ray-plus-reactor data shown in Fig. 4, except that a second dose-rate-independent component (''Population *C*'') was included to

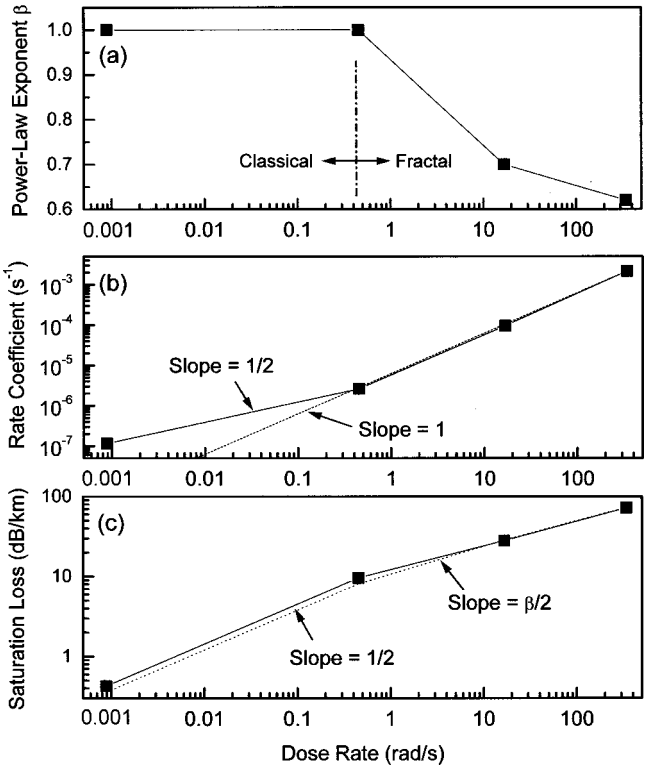

FIG. 5. Best-fit Population-*A* parametrizations of Eq. (17) [squares] used in the fits of the experimental data shown in Fig. 4. Population-*A* contributions were added together with that of a dose-rate-independent Population *B*, leading by cut-and-try procedures to the ''best fits'' illustrated in Fig. 4. In this case, the simulations were carried out under the notional constraint that the rate coefficient k and saturation loss N_{sat} should obey classical rules (i.e., slope $=1/2$) in the classical regime (i.e., in the low-dose-rate regime where $\beta=1$).

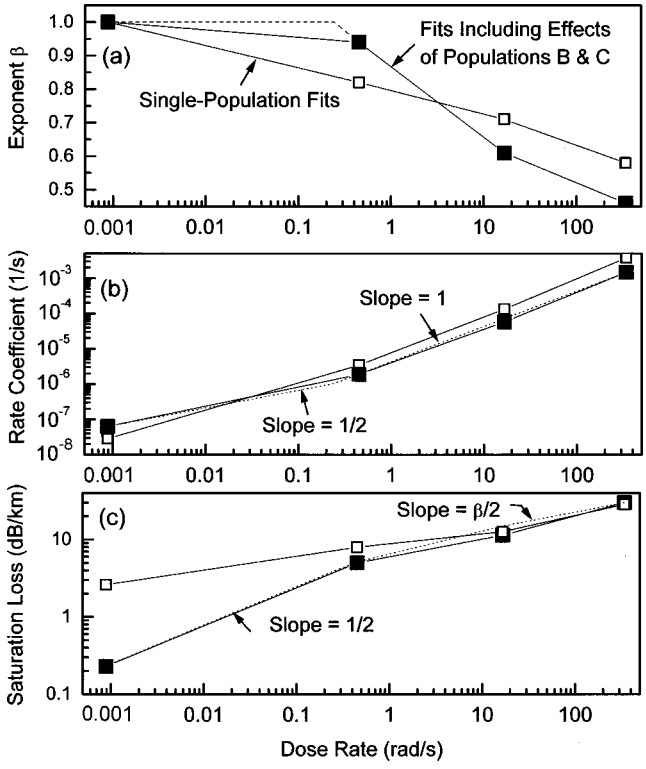

FIG. 6. Best-fit ''Population-*A*'' parametrizations of Eq. (17) [solid squares] used to fit the growth of optical attenuation at 1300 nm in Corning SM fibers subjected to γ irradiation at dose rates of 340, 17, and 0.85 rad/s and to reactor irradiation at 0.000 88 rad/s, all at 50 °C. These fits were carried out under the assumption that certain iteratively determined dose-rate-independent ''Populations *B* and *C*'' (not illustrated) also contributed to the experimental growth curves. Open squares represent best fits achieved without this assumption. (The experimental data for the γ-irradiated fibers only (i.e., excluding the reactor data) are shown in Fig. 7; however, the simulations using the parameters of the present figure are not illustrated there.)

improve the quality of the fits at high doses. The best-fit parameters resulting from this process (Fig. 6, solid squares) exhibit a good qualitative correspondence to the parameters of Fig. 5, which represent the fits of the MM data of Fig. 4. For comparison, the open squares in Fig. 6 correspond to the best fits (not shown) that were achieved without assuming either a Population *B* or a Population *C*.

The three highest-dose-rate curves for the SM fiber under irradiation (Fig. 7, solid curves) are similar to those for the MM fiber (Figs. 1 and 4), except that the induced attenuations are weaker by factors ~ 2 and the corresponding fitting exponents β are substantially smaller at each respective dose rate. The solid squares in Fig. 7 are the results of irradiation in the γ-ray air source. The particular fits shown in Fig. 7 were accomplished under the same philosophy as those of Fig. 4, namely, it was presumed that the weak contribution(s) of at least one dose-rate-independent defect population underlies the principal (dose-rate-dependent) induced absorptions that are here termed ''Population-*A*'' color centers. Thus, it was supposed that the ''correct'' choice of underlying dose-rate-independent component(s) would be the one that leads to Population-*A* fitting parameters falling into the same ''canonical'' form as exemplified by Fig. 5. Figure 8 (solid squares) shows the Population-*A* parameters used for the fits of Fig. 7; the Population-*B* and Population-*C* dose-rate-independent components also used in these fits are illustrated by the small solid circles in Fig. 7. For comparison, the open squares in Fig. 8 represent Population-*A* best fits (not shown) carried out without recourse to underlying components *B* or *C*.

Comparison of the trends defined by the solid squares in Fig. 6 with those of Fig. 8 reveals the influence of employing the reactor data in the former case and the γ-ray-air-source data in the latter case as the lowest-dose-rate ''anchor.'' By reliance on the reactor data, the fitting procedure leads in Fig. 6 to a fractal$\rightleftarrows$classical phase transition at a dose rate of ~ 0.25 rad/s for the SM fiber similar to that revealed in Fig. 5 for the MM fiber (which was similarly anchored at the lowest dose rate by reactor data). By contrast, use of the γ-ray-air-source data shown in Fig. 7 (solid squares) causes the apparent fractal$\rightleftarrows$classical transition to recede to a dose rate of ~ 0.01 rad/s (Fig. 8). Otherwise, there are no major differences between the fitting parameters of Figs. 6 and 8 (other than the slope$=1/2$ segments in Fig. 6 that are present by construction to force the fits to obey classical kinetics in

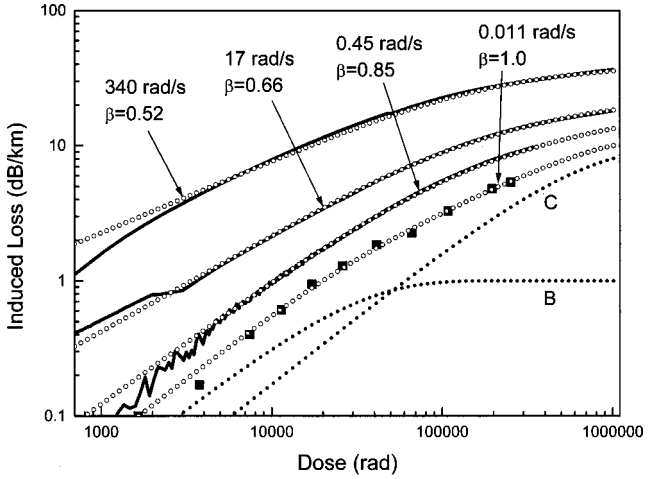

FIG. 7. Growth of induced attenuation at 1300 nm in Corning SM Ge-doped-silica-core fiber subjected to γ irradiation at dose rates of 0.011, 0.45, 17, and 340 rad/s at 50 °C. Solid curves and solid squares are the experimental data; small open circles are fits to these data based on the stretched second-order-kinetic growth solution, Eq. (17), using the ''Population-*A*'' parameters plotted in Fig. 8 as solid squares. All four fitted curves include the influences of dose-rate-independent ''Populations *B* and *C*'' (small solid circles) that were co-optimized in the cut-and-try fitting process.

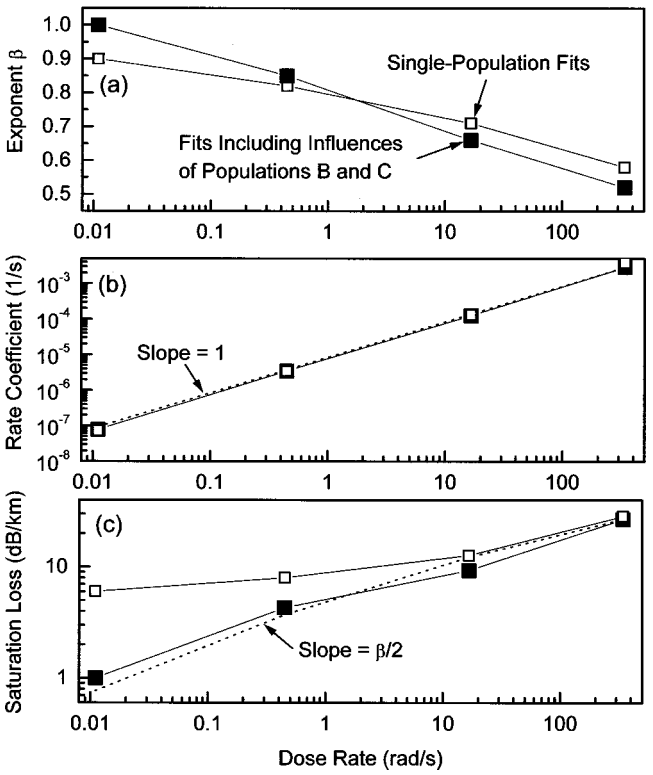

FIG. 8. Best-fit ''Population-*A*'' parametrizations of Eq. (17) used to fit the growth of optical attenuation at 1300 nm in Corning SM fibers subjected to γ irradiation at dose rates of 340, 17, 0.85, and 0.011 rad/s at 50 °C. The fits represented by the solid squares were carried out under the assumption that dose-rate-independent ''Population *B* and *C*'' also contribute to the experimental growth curves; these fits, together with the underlying ''Populations-*B*-and-*C*'' curves themselves are shown in Fig. 7. Open squares represent best fits (not illustrated) achieved without assumption of underlying dose-rate-independent components.

the classical regime). Thus, while one of the lowest-dose-rate data sets must be misleading (presumably the reactor data), the fitting procedures developed here are seen to be robust in their consistent ability to fit the higher-dose-rate data even when evoking dose-rate-independent Populations *B* and *C* that are (in at least one case) influenced by a false lowest-dose-rate ''anchor.'' Note in this regard that the ''bad'' data point at 17 rad/s in Fig. 6(c) (solid square falling below the dotted theory curve) is replicated in Fig. 8(c), thus exonerating ''anchor-point'' error from being its cause.

Thus, despite some imperfections, possibly related to systematic errors in the restricted data sets employed here, it is proposed that the functional relationships of the parameters plotted in Fig. 5 indeed define a canonical form for both first-and second-order kinetics in cases where there exists a fractal$\rightleftarrows$classical phase transition at a certain dose rate. Furthermore, it appears that all of the present growth data can be well fit by Eqs. (13) or (17) by use of discrete values of k, β, and N_{sat}.

B. Decay curves

Postirradiation decay curves were measured only for the MM and SM fiber coils exposed at the highest dose rate (340 rad/s). These data are plotted as the bold curves in Fig. 9. The dotted and dashed curves are the ''predicted'' stretched first- and second-order decay behaviors for the MM fiber obtained by taking the rate constants R and exponents β determined from the fits of the uppermost growth curves in Figs. 1 and 4 and plugging them into Eqs. (1) and (20), respectively. In the first-order case $R \equiv k$, whereas it can be shown that in the second-order case $R = k/(N_{\mathrm{sat}})^{1/\beta}$ (see Table I). On inspection of Fig. 9, it is apparent that the effective decay-rate constants R resulting from this naive approach are much too large; in fact, they exceed the best-fit value of R for the MM fiber decay curve by factors of $\sim$15 in both the first- and second-order cases. The exponents β of the growth curves are also large in comparison with the actual best-fit parameters of the decays. This outcome is understandable in terms of the heuristic deconstructions of power-law growth curves by Griscom, Gingerich, and Friebele[9] into summations of classical saturating nth-order-kinetic solutions wherein the dominant subpopulations at a given dose D_i are characterized by rate constants $K_i(D_i)$ and $R_i(D_i)$, both of which decline in magnitude for larger values of D_i. Specifically, it was shown[9] that R_i is proportional to D^{-1} in the first-order case and to $D^{-(\beta+1)}$ in the second-order case. Thus, while the fixed values of K and R implicit in the parametrization of Eqs. (13) and (17) represent a mathematical convenience in fitting experimental growth curves and facilitate extrapolation of the growth results to doses and dose rates outside of the ones employed in the experiment, the derived (time-independent) value of the parameter R cannot be used directly to predict the decay rate when the radiation is interrupted at an arbitrary time. Indeed, the characteristic decay times τ_c to be associated with *power-law* growth

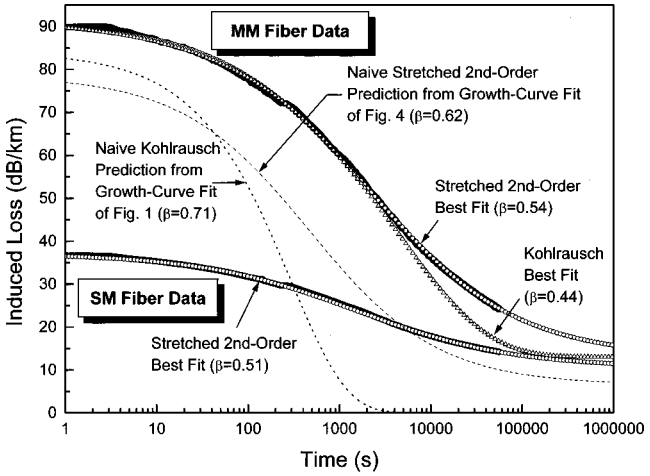

FIG. 9. Isothermal decay curves (50 °C) of γ-ray-induced attenuation in Corning MM and SM fibers following 1 Mrad irradiations at 340 rad/s. Small open symbols are best-fit simulations based on the Kohlrausch law, Eq. (1) (triangles), or stretched-second-order kinetics, Eq. (20) (circles). Dashed curves are naive no-adjustable-parameter predictions based solely on the parametrizations of fits of the growth curves shown in Figs. 4 and 7.

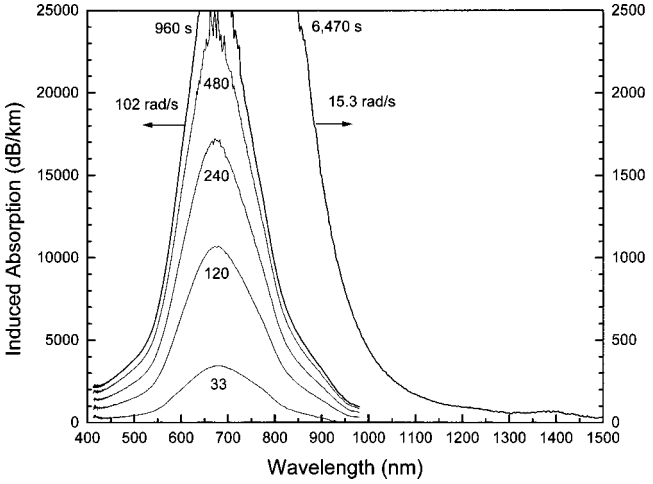

FIG. 10. γ-ray induced optical absorption bands in a fluorine-doped-silica-core optical fiber at 27 °C in the dark. Short-wavelength spectra were recorded on a prism-based CCD-camera spectrometer (irradiation times given in seconds) using a 1 m length of fiber in the radiation field at a dose rate of 102 rad/s. Long-wavelength spectrum was recorded on an optical signal analyzer using a 10-m irradiated length after 6470 s at 15.3 rad/s.

curves (exponent β) have been deduced to be[27] $\tau_c = t_{\text{irrad}}[(n-1)(1-\beta)]^{-1}$ for $n>1$ and $\tau_c = t_{\text{irrad}}/(1-\beta)$ for $n=1$, where t_{irrad} is the irradiation time. But even this simple rule does not apply in the present case, where growth curves are recorded in high-dose regimes where they no longer obey simple power laws.

The illustrated fits to the decay curves of Fig. 9 each involved three adjustable parameters, R, β, and N_∞ (the conjectural nondecaying component), since $N(0)$ is essentially given. The parameter N_∞, which might have been determined with greater confidence had decay data collection been extended to longer times, presumably corresponds to the cumulative dose-rate-independent components conjectured here to contribute to the growth curves. In the case of the MM fiber, the cumulative Population-B contribution of Fig. 4 was 7.3 dB/km, vis-à-vis $N_\infty \approx 13$ dB km used for the stretched-second-order fit of the decay curve of Fig. 9 (open circles). A discrepancy of this magnitude likely results from the omission of a ''population C'' in fitting the MM-fiber growth data of Figs. 1 and 4, in contrast to its inclusion in fitting the SM growth curves of Fig. 7. (A dose-rate-independent ''Population C,'' had it been employed, would have tended to compensate for the fitting discrepancies at highest doses in Fig. 4.) The Kohlrausch fit (open triangles) of the MM-fiber data of Fig. 9 arbitrarily employs the same value of N_∞ (13 dB/km) as for the stretched-second-order fit.

In the case of the SM fiber, the cumulative nondecaying Population-B-plus-Population-C contribution to the growth curve simulation of Fig. 7 was 10.6 dB/km, in excellent agreement with $N_\infty = 10.5$ dB/km used to fit the SM decay curve of Fig. 9 (only the second-order fit is shown). The best-fit values of β for the SM growth and decay curves were 0.52 and 0.51, respectively, again showing excellent agreement. However, the value of the decay rate constant R predicted from the growth curve was five times larger than the best-fit value for the decay curve, very likely for the reasons discussed above in the context of the MM fibers.

V. FRACTAL KINETICS OF COLOR-CENTER FORMATION AND BLEACHING IN PURE AND F-DOPED SILICA-CORE OPTICAL FIBERS

A. Results of continuous irradiation in the dark

Figure 10 presents some spectral data typical of γ-ray-induced color centers (believed to be self-trapped holes)[20,21] in both pure and fluorine-doped silicas having very low hydroxyl and chloride contents; (the illustrated bands are suppressed in otherwise pure silicas with elevated levels of OH or Cl).[19] The actual data displayed in Fig. 10 pertain to the F-doped-silica-core fiber and show the initial growth of color-center absorption bands recorded *in situ*. Elapsed times since the start of the irradiation are given in seconds in the case of the spectra acquired by means of the prism-CCD-camera spectrometer at 102 rad/s. The spectral trace extending to longer wavelengths was acquired by an OSA after a period of 6470 s at a dose rate of 15.3 rad/s. (resulting in approximately the same dose as 960 s at 102 rad/s). Because the lengths of fiber in the radiation field were 1 and 10 m for the short- and long-wavelength measurements, respectively, the maximum loss that could be reliably measured was lower by an order of magnitude in the latter case.

Figure 11(a) (solid triangles) shows the kinetic behavior of the induced absorption in the F-doped-silica-core fiber measured at a fixed wavelength of 670 nm corresponding approximately to the peak of the absorption. No attempt was made to resolve the data into separate absorption bands. However, Gaussian resolutions of distinct bands centered at 660 and 760 nm in a low-OH/low-Cl pure-silica-core fiber were earlier performed by Nagasawa, Tanabe, and Yahgi,[4] whose results are replotted at the bottom of Fig. 11(a). It is

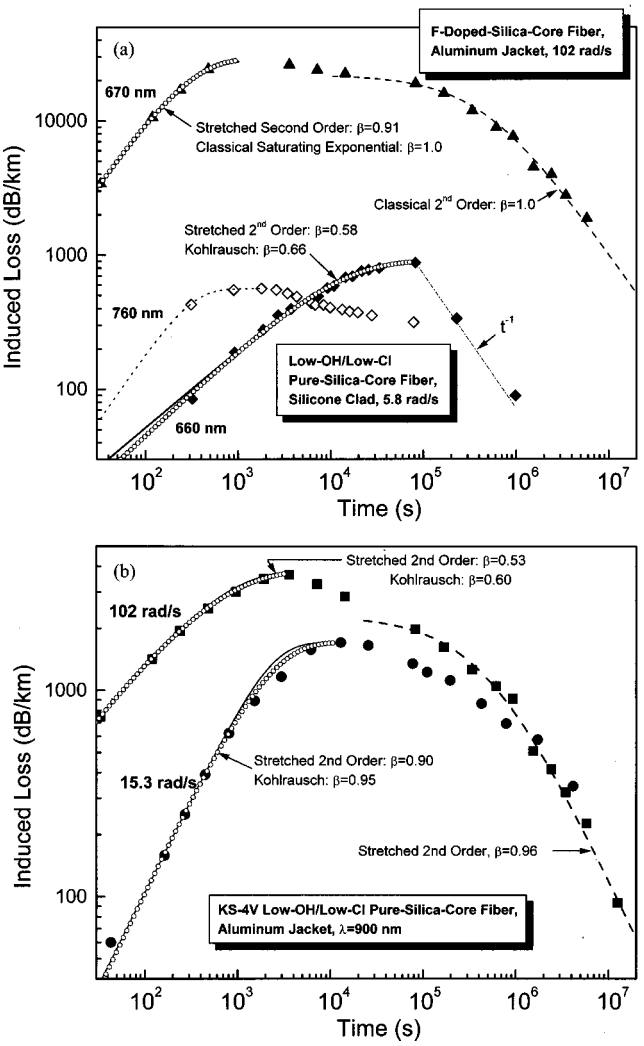

FIG. 11. Growth and radiation-stimulated destruction of optical absorption in silica-based fibers γ-irradiated in the dark at room temperature. (a) F-doped-silica-core, Al-jacketed fiber measured at 670 nm (top) and Gaussian resolutions[4] of bands peaking at 660 and 760 nm in a low-OH/low-Cl pure-silica-core, polymer-clad fiber (bottom). (b) Low-OH/low-Cl KS-4 V pure-silica-core, Al-jacketed fiber measured at 900 nm. Fitted growth curves are based on Eqs. (13) and (17) (open circles and solid curves, respectively). The short dashed curve in (a), also based on Eq. (13), is intended as a suggestive guide to the eye.

clear from these data that the 760-nm band was primarily responsible for the initial absorption in Nagasawa's fibers; (the same band is clearly present in the spectra of Fig. 10 but is considerably weaker than the 660-nm band at all times $\geqslant$33 s). According to Nagasawa's deconvolution, the 760-nm band rises to its maximum intensity in a time $\sim$1000 s and declines with continuing irradiation thereafter. This band therefore represents a chemical intermediate which, even while being created, is being converted into further products. Therefore, it is purely for heuristic purposes that the growth stages of all curves in Fig. 11 have been fitted with saturating Kohlrausch and stretched-second-order functions, i.e., Eqs. (13) (small open circles) and (17) (solid curves), respectively. Again benefitting from Nagasawa's Gaussian resolutions,[4] it is seen that the 660-nm band grows more slowly and with more highly stretched kinetics ($\beta\sim0.6$) relative to the 760-nm band ($\beta\sim0.9-1.0$); the 660-nm band reaches quasisaturation in times $\sim10^5$ s. Thus, the 660-nm band may in fact be the spectroscopic signature of one of the products of the reaction that consumes the color centers responsible for the 760-nm band.

a. Radiation-stimulated reconfiguration. At longer times a very different phenomenon is encountered; namely, the numbers of induced color centers absorbing at all wavelengths decrease according to classical, or near-classical, second-order kinetics (see bold long-dashed curves fitted to the long-time data in Fig. 11). We shall refer to this phenomenon as ''radiation-stimulated reconfiguration (RSR),'' since the structural configurations in the glass favorable to trapping radiation-generated free carriers are progressively removed as the radiation continues for long times.[20,21]

Kinetic data for the low-OH/low-Cl KS-4V pure-silica-core fiber are presented in Fig. 11(b). These data were extracted at a fixed wavelength of 900 nm in order to stay within the dynamic ranges of both the long- and the short-wavelength measurements (see Fig. 10). The qualitative features of these data are very similar to those that characterize the peak of the absorption curve near 670 nm extracted from the same spectra (not shown here) and they also resemble the 670-nm data for the F-doped-core fiber shown in Fig. 11(a). It is seen in Fig. 11(b) that the RSR curves for the two different dose rates become confluent for times greater than $\sim10^6$ s. Thus *the RSR process depends on time, rather than dose*. This peculiar phenomenon has been noted previously at three different dose rates;[20] however, the data of Fig. 11(b) represent the first time that two virgin fibers from the same spool with no previous radiation histories were irradiated at two widely separated dose rates ''in the dark'' for the full term of the experiment (ignoring the $\sim$2–5 s illuminations per frame grab or $\sim$20 s per OSA scan).

The presumptive reason why the initial data point in the lower-dose-rate data set in Fig. 11(b) (filled circles) falls to the left of the fitted growth curve is that the time marker was taken as the start of the OSA scan, rather than the time when the scan reached 900 nm. A more serious inconsistency bears particular mention, namely, the abrupt breakoff to a t^{-1} behavior displayed by the 660-nm band of Nagasawa, Tanabe, and Yahgi[4] [Fig. 11(a)] at an irradiation time two orders of magnitude shorter than for the other data portrayed in Fig. 11. It is suggested that Nagasawa's data were truncated by action of radiolytic atomic hydrogen created in the silicone optical cladding of his fiber that then diffused into the fiber core where it reacted with the induced color centers. A precedent for such a process has been established.[11] The aluminum-jacketed fibers of the present study were immune to such effects—and also to inadvertent bleaching by room light entering laterally.

The RSR phenomenon has been shown to be independent of dose rate over a range $\sim$15–550 rad/s. It is therefore presumed to be thermally activated above a certain threshold dose rate $\leqslant$15 rad/s. That is, suprathreshold irradiations can be viewed as ''switching on'' the process. Because the process appears to be second order, it can be either of the type

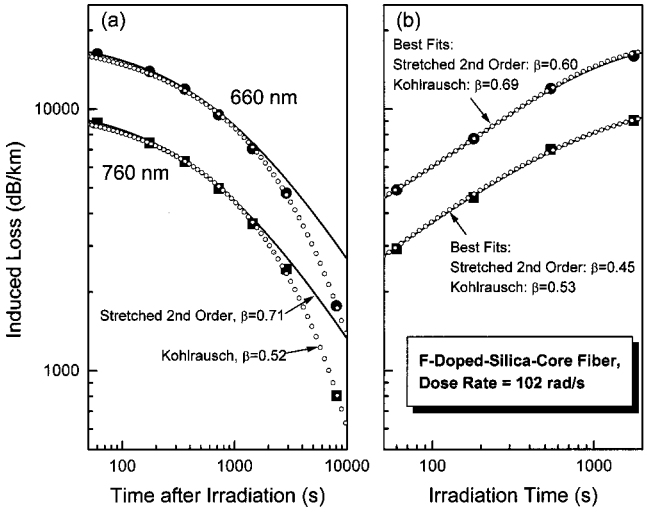

FIG. 12. γ-ray-induced optical absorption measured at 660 and 760 nm (large symbols) in a fluorine-doped-silica-core optical fiber at 27 °C in the dark: (a) isothermal decay as a function of time following removal from the radiation source and (b) regrowth as a function of time following reinsertion into source. Fitted curves are based on Eqs. (13) and (17) [small open circles and solid curves, respectively]; the same values of β were used for both of the fits in (a).

$X+X\rightarrow$products or $X+Y\rightarrow$products, where the initial concentrations of X and Y are equal. Some examples of the latter type might be electrons and holes or vacancies and interstitials. However, irradiation replenishes free electron-hole pairs at a constant rate, while additional vacancy-interstitial pairs continue to be created in silica glasses with each increment of dose up to total doses exceeding those of the present experiments by four orders of magnitude.[28] Therefore, neither recombination of free electrons and holes nor recombinations of vacancies and interstitials can account for steadily decreasing color-center populations in the present situation. However, models based on specific types of electron- or hole-*trapping sites* that decrease in number with increasing dose are not eliminated from consideration. Indeed, it has previously been proposed[20] that the optical bands in question are due to carriers trapped on strained bonds and that these trapping sites are monotonically reduced in number with increasing radiation time by dimerization, i.e., by an $X+X$ type reaction. This model envisions that strained bonds in silica glass are mobilized by ionizing irradiations exceeding a certain threshold dose rate, yet to be determined. More specifically, it was supposed that such strained bonds are preferential hole-trapping sites that result in Anderson localized holes.[21,29] Thus, reconfigurations of the silica glass network that lower the number of strained bonds may be connected with a decrease of the density of states lying between the top of the valence band and the mobility edge for hole transport.

B. Thermal and optical bleaching and regrowth

a. Thermal bleaching. The data points in Fig. 12(a) represent the isothermal decay of the γ-ray-induced optical bands in the F-doped-silica-core fiber upon its withdrawal from the source 82 800 s after the start of the irradiation at 102 rad/s. Figure 12(b) shows their regrowth upon reinsertion of the sample coil into the source. The data were taken from the raw spectra at 660 and 760 nm without performing Gaussian resolutions. As in Fig. 11, the experimental data (large solid symbols) were fitted by formalisms presented above (small open circles for stretched exponential formulas and solid lines for stretched second-order expressions). By construction, each fitted curve passes through the point at $t=0$ (which cannot be shown on the log-log plots); the ultimate points in Fig. 12(a) are in fact the zero-time points for the data of Fig. 12(b). Because of the leverage of the zero-time point, efforts to better fit the long-time points may result in poorer fits of the point corresponding to the shortest nonzero time. Thus, the stretched second-order expression, Eq. (20), could be made to fit the *pen*ultimate long-time point at the expense of passing slightly above the shortest-time point. But in no event could the *ultimate* points in the decay curves be fit by Eq. (20). On the other hand, the stretched exponential (Kohlrausch) function, Eq. (1), can be made to fit all of the long-time points rather well. Nevertheless, the best Kohlrausch fit passes noticeably below the shortest-nonzero-time point. It is suggested here that the decay process involves recombination of electrons and holes. Thus, it is proposed that second-order kinetics should govern short times when self-trapped carrier concentrations are high and randomly distributed throughout the glass, while the behavior at long times may reflect the onset of pseudo-first-order kinetics as the remaining recombinations increasingly involve isolated coulombically-bound e-h pairs. Accordingly, in Fig. 12(a) the stretched-second-order fits have been optimized on the short-time points, while the Kohlrausch fits were optimized on the long-time points. So far as these fits were concerned, the decay kinetics measured at 660 and 760 nm were indistinguishable. By contrast, upon resumption of the irradiation, the regrowth curve determined at 760 nm proves to be considerably more stretched than the curve measured at 660 nm [Fig. 12(b)].

b. Optical bleaching. The optical bands illustrated in Fig. 10 are readily bleached by white light. Figure 13(a) displays the bleaching kinetics measured at 670 nm for two different fibers (KS-4V-silica core, squares; F-doped-silica core, circles) each studied at two different dose rates (535 rad/s, solid symbols; 25 rad/s, open symbols) during continuous injection of ~ 5 μW of white light commencing $\sim 1\frac{1}{2}$ days after the sample coils were inserted into the radiation source. Again, these curves have been fitted by Eqs. (13) and (17) (small open circles and continuous curves, respectively). The curves are sigmoidal because the induced losses are finite both at $t=0$ (the start of the illumination) and at long times, since the destruction of trapped carrier centers by light (and by collateral thermal processes) will approach equilibrium with the creation of new centers by γ rays at long times. Since the formalisms presented in Sec. II do not include an optical destruction mechanism, for present purposes we have approximated the expected kinetics in the form $N(t)=N(0)-N^n(t)$, where $n=1$ and $n=2$ refer to Eq. (13) or to Eq. (17), respectively. The coefficients $k^{(n)}$ and $N_{\rm sat}^{(n)}$ clearly must depend on light intensity, but this dependence has not

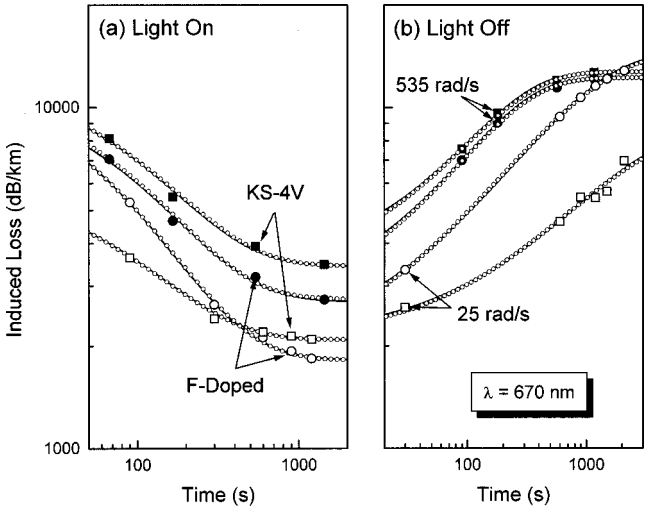

FIG. 13. Isothermal white-light bleaching kinetics of pure (KS-4V) and F-doped silica-core fibers measured at 670 nm during uninterrupted γ irradiation: (a) as a function of time following commencement of 5-μW illumination and (b) as a function of time following extinction of the bleaching light. Fitted curves are based on Eqs. (13) and (17) [small open circles and solid curves, respectively]. The values of β pertaining to the fitted curves for KS-4V in (a) were independent of dose rate and equal to 0.67 and 0.55 for the first- and second-order fits, respectively; those for the F-doped silica were about the same at the 535 rad/s but dropped to 0.58 and 0.48, respectively, at the lower dose rate. For the ''regrow'' curves of (b), the fitted values of β were identical for the two types of silica but were dose-rate dependent: $\beta=0.83$ and 0.71, respectively, for the first- and second-order fits at 535 rad/s and $\beta=0.66$ and 0.58, respectively, at 25 rad/s.

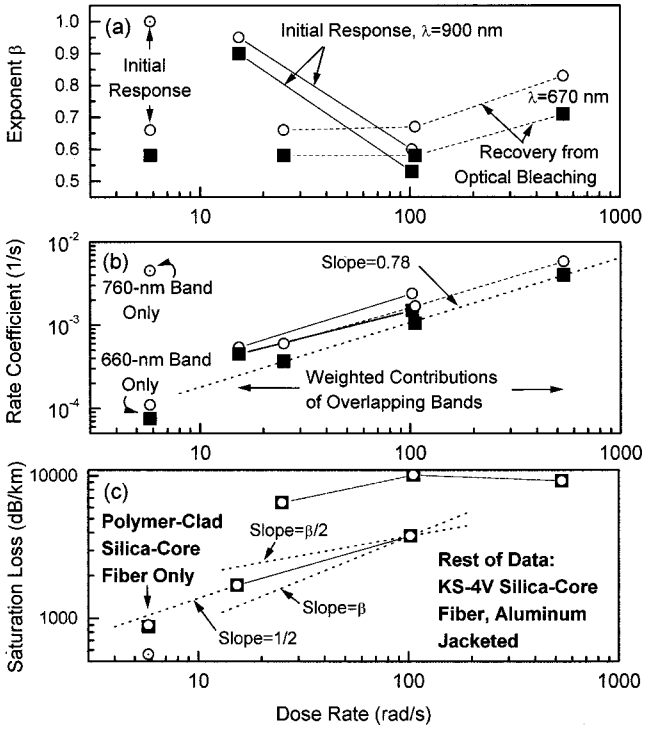

FIG. 14. Best-fit parametrizations of Eqs. (13) [open circles] and (17) [solid squares] used in simulations of some of the experimental growth data of Fig. 11 and the regrowth data of Fig. 13(b) augmented by additional regrowth data at 105 rad/s (not shown). Data at the lowest dose rate are for the low-OH/low-Cl pure-silica-core, silicone-clad fiber of Ref. 4; all others pertain to low-OH/low-Cl KS-4V pure-silica-core, Al-jacketed fiber. Solid and dashed straight lines connect points acquired under identical conditions other than dose rate. Dotted lines represent specific power-law behaviors discussed in the text.

yet been investigated. The recovery kinetics when the bleaching light was switched off are shown in Fig. 13(b).

b. Fractal kinetics of metastable color center formation in pure fused silica. Some of the parameters used in the kinetic fits of Figs. 11 through 13 have been plotted in Fig. 14, where all of the annotations in any given panel (with the exceptions of the slopes of straight lines drawn for guidance) pertain to the other two panels as well. Thus, all of the data plotted at a dose rate of 5.8 rad/s belong to Nagasawa's silicone-clad, OH-free/low-Cl pure-silica-core fiber for which the kinetics of bands at 660 (○, ■) and 760 nm (⊙) were separately determined by performing Gaussian resolutions.[4] The rest of the data pertain to metal-jacketed, F-doped-silica-clad, OH-free/low-Cl KS-4V pure-silica-core fibers and effectively represent weighted contributions of Nagasawa's two bands (and perhaps others) picked off at fixed wavelengths of 670 nm (data of Fig. 13) or 900 nm (data of Fig. 11) without performing spectral resolutions. Nagasawa's data of Fig. 11(a) and those of Fig. 11(b) represent the initial radiation responses of separate virgin fiber samples for each dose rate. By contrast, the data of Fig. 13 were recorded using a single fiber sample of each type (KS-4V and F-doped), both of which were subjected to successive irradiations at three progressively larger dose rates (only two of which are illustrated in Fig. 13). Each time the dose rate was changed and the irradiation had progressed for an additional $1-1\frac{1}{2}$ days (with the injected light turned off for the final 10–20 h), the fiber was subjected to continuous optical bleaching *in situ* for times up to ~12 h and was then monitored during the ''regrow'' of γ-ray-induced absorptions when the bleaching light was switched off. Thus, Fig. 14 combines the results of initial irradiations of virgin fibers in darkness at 900 nm with regrowth data obtained at 670 nm following *in situ* optical bleachings of fibers that were subjected to sequential irradiations at three increasingly greater dose rates. As per the convention established in earlier figures, circles represent stretched first-order kinetic fits and squares represent stretched second-order fits.

It can be seen in Fig. 14(a) that the long-wavelength ''initial response'' data (Nagasawa's 760-nm band[3,4] and the present 900-nm data) define a trend of β decreasing from the classical case ($\beta=1$) at the lowest dose rate to decidedly more fractal values at higher dose rates, fully congruent with the dose rate dependences of the corresponding parameters for the induced absorption at 1300 nm in the Ge-doped-silica-core fibers of Sec. IV. By contrast, Nagasawa's initial-response data for the 660-nm band[4] and the present regrowth-following-optical-bleaching data at 670 nm define a counter trend, exhibiting decidedly fractal behavior at the lower dose rates and a tendency towards more classical behavior at the highest dose rate. On the other hand, in Fig. 14(b) *all* rate-coefficient data for the pure-silica-core fibers

(both initial response and regrowth), appear to depend on dose rate approximately as $\dot{D}^{0.78}$ in the fractal regime—as opposed to the linear dependence seemingly revealed by the Ge-doped fibers in Figs. 2, 3, 5, 6, and 8. Moreover, the values of N_{sat} plotted in Fig. 14(c) deviate from the slope-$\beta/2$ behaviors that have seemed to characterize the color centers induced in the Ge-doped fibers. At this juncture, it is not possible to say whether the results for the pure-silica-core fibers imply that the putative ''canonical forms'' for the dose-rate dependences of k and N_{sat} inferred in Sec. IV in fact depend to some degree on material type or they are artifactual. That is, if the data of Fig. 14 are accepted at face value, the canonical rules could be $k \propto \dot{D}^{0.75}$ and $N_{sat} \propto \dot{D}^{0.75\beta}$, at least in the case of pure silica.

One argument favoring the ''new'' rules of Fig. 14 is that there seem to have been no underlying dose-rate-independent color-center populations in the pure-silica-core fibers whose effects must be taken into account. It is cautioned, however, that whereas application of Eqs. (13) and (17) to color centers in the Ge-doped-silica-core fibers appears fully justified, the use of these formalisms to fit the initial response curves of the pure-silica-core fibers was undertaken for purely heuristic reasons in the full knowledge that they do not fit the subsequent turnover and decline of the induced absorptions, particularly as regards the 760-nm band (see Fig. 11). Furthermore, it is conceivable that irradiation of virgin samples for each differing dose rate might have yielded results different from those of the present case where single fibers were subjected to sequential irradiations at successively larger dose rates. (Indeed the decline in N_{sat} apparent at the highest dose rate in Fig. 14(c) is likely to be attributable to the RSR effect discussed in Sec. V A.) Thus, in order to settle these questions, additional data for pure-silica-core fibers should be acquired under more controlled conditions, and the ''stretched kinetic'' analyses should be extended to coupled systems of differential equations that must account for both the rise and fall of the 760-nm band seen in Fig. 11(a).

VI. DISCUSSION

The Kohlrausch law of Eq. (1) has sometimes been described as ''universal,'' given its apparent applicability to an immensely broad range of relaxation phenomena in disordered materials. However, whereas Eq. (1) is derived from standard first-order kinetics by an appropriate change of dimensionless variable, analogous solutions that can be derived from second-order kinetics may prove more appropriate to bimolecular reactions taking place in fractal spaces. Specifically, stretched-second-order formalisms for the growth of color centers in insulating glasses under irradiation, Eq. (17), and for their thermal decay when the samples are removed from the radiation field, Eq. (20), have been presented and tested against actual experimental data.

In many cases illustrated above, successful simulations of color-center growth curves have been achieved using both the saturating stretched-exponential (Kohlrausch-type) solution and the present saturating stretched-second-order formalism, Eq. (17). In such cases, the best-fit exponents β have invariably been higher when using the Kohlrausch-type solution, Eq. (13), than when using Eq. (17) (see, e.g., Figs. 2 and 14). However, as demonstrated formally [and illustrated by the *calculated* solutions of Fig. 15(a)], the *same* value of β must be used in *both* formalisms in order to fit any data that approximate to power laws at very low doses. Thus, in the absence of data acquired at sufficiently low doses (which would reveal the true value of β), Eq. (13) can be made to approximate Eq. (17), or vice versa, by use of a false value of β. From inspection of Fig. 15, it appears that the true kinetic order governing color center creation and decay can be inferred from experimental growth and decay data, provided that such data extend to low enough doses and that they are uncontaminated by interfering components such as the dose-rate-independent components inferred to contribute to the induced optical absorption in Ge-doped-silica-core fibers measured at 1300 nm (see Figs. 4 and 7).

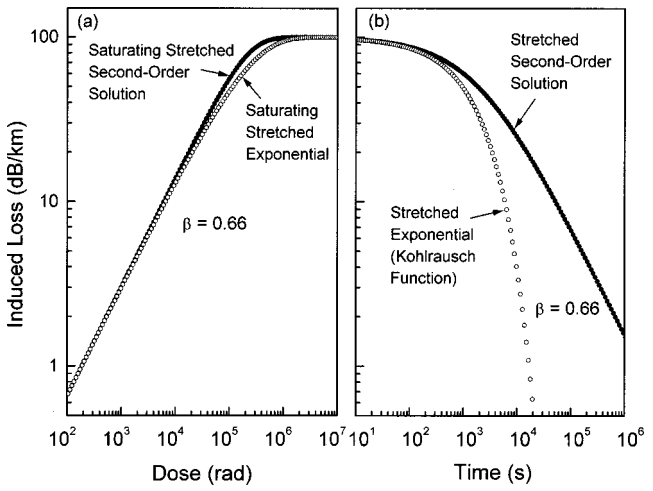

FIG. 15. Calculated stretched first- and second-order-kinetic solutions [Eqs. (13) and (17), respectively] for (a) color-center growth during irradiation and (b) their decay upon removal from the radiation source. The exponent β is arbitrarily selected to be 0.66 in all cases.

For lack of data recorded at sufficiently low doses, the present simulations of the growth curves for radiation-induced color centers in Ge-doped-silica glasses (Figs. 1, 4, and 7) do not clearly reveal the correct kinetic order of the decay mechanism. However, they do unveil some surprising and potentially useful empirical rules that *independently of kinetic order* appear to govern the dose-rate dependences of the underlying rate coefficients in the fractal regime (see Table I). A limited amount of data presented for radiation-induced color centers in *pure* silica glasses currently appears to lead to somewhat different rules. Additional work will likely be necessary to determine whether or not the material nature of the fractal structure indeed affects the parametrization of these new rules. Any such follow-on studies would necessarily include derivations of stretched-kinetic formalisms for higher-order chemical reactions and/or systems of coupled first-and second-order reactions as may be appropriate to the clearly more complex kinetics of radiation-induced color center (self-trapped hole?) formation in pure silica glasses that are particularly free of OH and chloride impurities (see Fig. 11).

ACKNOWLEDGMENTS

M. E. Gingerich, M. Putnam, W. D. Mack, and G. M. Williams are acknowledged for their gathering of the large body of data from which the presently treated Ge-doped-silica-fiber radiation-response curves were selected as typical. E.J. Friebele is thanked for his guidance and support of this work.

*Present address: Hosono Transparent Electro-Active Materials Group, Materials and Structures Laboratory, Tokyo Institute of Technology, 4259 Nagatsuta-cho, Midodi-ku, Yokohama 226-8503, Japan. Email address: dlgriscom@netscape.net

[1] E. J. Friebele, Opt. Eng. **18**, 552 (1979).
[2] E. M. Dianov, L. S. Kornienko, E. P. Nikitin, A. O. Rybaltovskii, and P. V. Chernov, Sov. J. Quantum Electron. **11**, 1171 (1981).
[3] K. Nagasawa, M. Tanabe, K. Yahagi, A. Iino, and T. Kuroha, Jpn. J. Appl. Phys. **23**, 606 (1984).
[4] K. Nagasawa, M. Tanabe, and K. Yahgi, Jpn. J. Appl. Phys. **23**, 1608 (1984).
[5] E. M. Dianov, V. N. Karpechev, L. S. Kornienko, A. O. Rybaltovskii, and P. V. Chernov, Sov. J. Quantum Electron. **14**, 1637 (1984).
[6] W. Schneider, U. Babst, H. Henschel, O. Kohn, and H. U. Schmidt, Proc. SPIE **721**, (1986).
[7] R. H. West, J. Lightwave Technol. **LT6**, 155 (1988).
[8] E. J. Friebele, M. E. Gingerich, and D. L. Griscom, Proc. SPIE **1791**, 177 (1992).
[9] D. L. Griscom, M. E. Gingerich, and E. J. Friebele, Phys. Rev. Lett. **71**, 1019 (1993).
[10] H. Henschel and E. Baumann, J. Lightwave Technol. **LT14**, 724 (1996).
[11] O. Deparis, D. L. Griscom, P. Mégret, M. Decréton, and M. Blondel, J. Non-Cryst. Solids **216**, 124 (1997).
[12] A. I. Gusarov, A. V. Dmitryuk, A. N. Konov, and V. A. Mashkov, Sov. Phys. JETP **70**, 289 (1990).
[13] R. Kohlrausch, Ann. Phys. (Leipzig) **12**, 393 (1847).
[14] G. Williams and D. C. Watts, Trans. Faraday Soc. **66**, 80 (1970).
[15] K. L. Ngai, Comments Solid State Phys. **9**, 127 (1979); **9**, 141 (1979).
[16] R. G. Palmer, D. L. Stein, E. Abrahams, and P. W. Anderson, Phys. Rev. Lett. **53**, 958 (1984); **54**, 1956 (1985).
[17] V. A. Mashkov, W. R. Austin, L. Zhang, and R. G. Leisure, Phys. Rev. Lett. **76**, 2926 (1996).
[18] E. J. Friebele, G. M. Williams, and W. D. Mack, Proc. SPIE **3848**, 232 (1999).
[19] D. L. Griscom, J. Appl. Phys. **80**, 2142 (1996).
[20] D. L. Griscom in *Defects in Insulating Materials*, edited by G. T. Matthews and R. T. Williams (Materials Science Forum, 1977), Vols. 239–241, pp. 19–24.
[21] D. L. Griscom, Appl. Phys. Lett. **71**, 175 (1997).
[22] R. Kopelman, Science **241**, 1620 (1988).
[23] J. Klafter and M. Shlesinger, Proc. Natl. Acad. Sci. U.S.A. **83**, 848 (1986).
[24] B. B. Mandelbrot, *The Fractal Geometry of Nature* (Freeman, San Francisco, 1983).
[25] R. Kopelman, J. Stat. Phys. **42**, 185 (1986).
[26] S. Alexander and R. Orbach, J. Phys. (Paris) **43**, L625 (1982).
[27] D. L. Griscom, M. E. Gingerich, and E. J. Friebele, IEEE Trans. Nucl. Sci. **41**, 523 (1994).
[28] R. L. Pfeffer, J. Appl. Phys. **57**, 5176 (1985).
[29] D. L. Griscom, J. Non-Cryst. Solids **149**, 137 (1992).